Onset of diffuse reflectivity and fast electron flux inhibition in 528-nm-laser–solid interactions at ultrahigh intensity

T. Feurer, W. Theobald, and R. Sauerbrey
Institut für Optik und Quantenelektronik, Friedrich-Schiller-Universität, Max-Wien-Platz 1, D-07743 Jena, Germany

I. Uschmann, D. Altenbernd, U. Teubner, P. Gibbon, and E. Förster
Max-Planck-Arbeitsgruppe Röntgenoptik an der Friedrich-Schiller-Universität, Max-Wien-Platz 1, D-07743 Jena, Germany

G. Malka and J. L. Miquel
Commissariat a l'Energie Atomique, Centre d'Etudes de Limeil-Valenton, 94195 Villeneuve-Saint-Georges Cedex, France
(Received 19 March 1997)

Using a high-power femtosecond frequency-doubled Nd:glass laser system with a contrast ratio of 10^{12}, the interaction between light and matter up to intensities of 10^{19} W cm^{-2}has been investigated. The absorption of the laser light in solid aluminum is almost independent of the polarization, peaks at about 25°, and reaches values of almost 45%. Assuming an exponential electron distribution, a temperature of 420 keV at 4×10^{18} W cm^{-2}was measured. These experiments and the detection of the hard-x-ray radiation (60 keV–1 MeV) implied a conversion efficiency of 10^{-4}–10^{-3} into suprathermal electrons. A second low-energy electron distribution either with trajectories mainly parallel to the target surface or with a reduced penetration depth due to flux inhibition was also inferred from $K\alpha$ line radiation measurements. [S1063-651X(97)08209-3]

PACS number(s): 52.40.Nk, 52.25.Nr, 52.50.Jm, 32.30.Rj

I. INTRODUCTION

Over the past few years there has been considerable progress in the development of femtosecond high-power laser systems. These devices offer the posibility to create plasmas with high electron densities and short scale lengths using relatively moderate laser energies. One possible application of such lasers to inertial confinement fusion is the recently proposed ''fast ignitor'' [1]. The basic idea of this scheme is to seperate the compression phase from fuel ignition that leads to lower requirements on the drivers. After compressing the fuel by several hundred-fold, the fuel is ignited by a burst of electrons that are created by an intense subpicosecond laser pulse. In order to characterize the efficiency of the processes involved and to obtain an estimate of the laser parameters that are required for the fast ignitor concept, it is necessary to determine the efficiency of the absorption process and the production of suprathermal electrons.

High-intensity ultrashort laser pulse absorption has been studied extensively both experimentally and theoretically for laser pulses of different wavelengths ranging from 0.25 μm (KrF laser) to 1.06 μm (Nd:glass laser) [2–13]. The absorption depends on several parameters, such as laser wavelength, intensity, pulse duration, polarization, or angle of incidence. Furthermore, the intensity of the laser pulse has a strong influence on the mechanisms of the laser-plasma interaction. For instance, at intensities below 10^{16} W cm^{-2} the dominant absorption process is collisional absorption, though resonance absorption may also play an important role [3,5,14]. The situation changes drastically at intensities exceeding 10^{17} W cm^{-2} and, in particular, at oblique incidence. Here the plasma becomes collisionless and collective absorption mechanisms such as the Brunel effect [9,11] and the anomalous skin effect [15,16] become dominant. One-dimensional simulations, with particle-in-cell (PIC) codes [11,13] or Vlasov simulations [16], are in good agreement with experimental results in this intensity range [17]. However, at ultrahigh intensities ($>10^{19}$ W cm^{-2}) additional high-intensity effects, such as surface modifications by hole boring [18], other surface instabilities, and relativistic effects, may influence the absorption physics.

Suprathermal electrons can be produced by several mechanisms, such as resonance absorption at the critical density for p-polarized light [3,5,9,11]. Other sources of suprathermal electrons can be parametric instabilities, e.g., Raman scattering or two-plasmon decay. Electron parametric instabilities driven by femtosecond pulses propagating in a plasma of arbitrary density have been studied in detail by Quesnel *et al.* [19]. For laser intensities where the quiver energy equals or even exceeds the electron rest energy m_ec^2, relativistic effects become important. Now magnetic fields are no longer negligible and the longitudinal component of the Lorentz force accelerates electrons parallel to the laser wave vector [18]. PIC simulations have shown that the hot-electron temperature k_BT_h is approximately the quiver energy E_{quiv}; therefore,

$$k_BT_h \approx m_ec^2[\sqrt{1+7.28\times10^{-19}(I\lambda^2)}-1], \qquad (1)$$

where $I\lambda^2$ is in units of W cm^{-2} μm^2. For $I\lambda^2=2\times10^{18}$ W cm^{-2} μm^2 a temperature on the order of 250 keV is obtained. Recent experiments in the ultra–intense relativistic regime with $I\lambda^2>10^{19}$ W cm^{-2} μm^2 have confirmed this suprathermal electron scaling law with laser intensity, and temperatures of up to 1 MeV have been measured [20].

The purpose of the present experiments is the investigation of the interaction of a light pulse of high contrast ratio (10^{12}) and high intensity ($>10^{19}$ W cm^{-2}) with solid targets. Of particular interest is the extension of our previous absorption experiments [5,17] to higher intensities, the effect

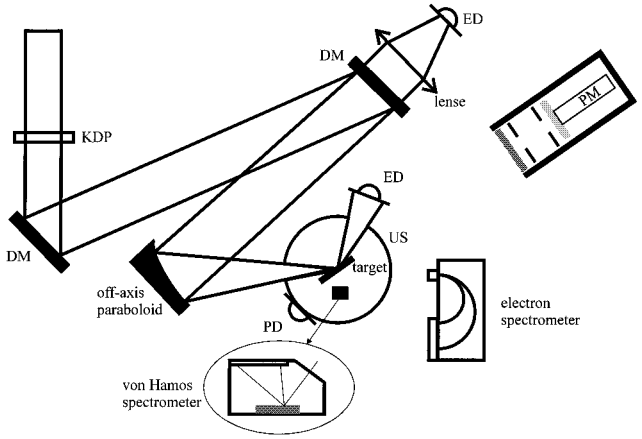

FIG. 1. Experimental setup. After the doubling crystal (KDP) the beam is reflected by two dielectric mirrors (DM) plus an off-axis paraboloid before impinging on the target. For the absorption measurements the back reflected and the specular reflected light is measured with energy detectors (ED); the diffuse reflected light is collected by an Ulbricht sphere (US) and measured with a photodiode (PD) that was equipped with color glass filter to discriminate plasma radiation. For the characterization of the suprathermal electrons the Ulbricht sphere is removed and three detectors are used simultaneously: an electron spectrometer, a von Hamos spectrometer, and a pair of scintillators attached to photomultipliers (PM).

of the ponderomotive force on the plasma surface, the determination of temperature and production efficiencies of the fast electrons, as well as the detection of hard x rays.

II. EXPERIMENTAL PROCEDURE

The experiments were performed with the P102 laser at CEA/L-V in Limeil [22]. Using the chirped pulse amplification scheme, the laser delivers up to 30 J in about 350 ± 50 fs (assuming a Gaussian intensity profile) at 1056 nm. The laser pulse is subsequently frequency doubled by a potassium dihydrogen phosphate (KDP) crystal (528 nm), reaching a maximum conversion efficiency of about 25% (see Fig. 1). The repetition rate was one shot every 20 min and the shot-to-shot fluctuations in energy were below 10%. The contrast ratio was better than 10^{12}, so even at the highest intensities, no preplasma is created on the target surface before the main pulse. The contrast ratio was measured for the fundamental wavelength using an autocorrelator (<10 ps), a crosscorrelator (<100 ps), and a fast photodiode (>100 ps) and was found to be on the order of 10^8. After the doubling crystal there are three dicroic mirrors (including the off-axis parabola), each having a reflectivity of about 95% for the second harmonic and about 4% for the fundamental; therefore, the total contrast ratio is better than 10^{12}. The pulses were focused using an off-axis parabola ($f/3$) leading to a minimum focal spot size of 5 μm full width at half maximum. The spatial intensity distribution in the focal plane was measured by a microscope objective leading to a magnified image that was subsequently recorded by a charge coupled device camera. The central spot contained about 15% of the full energy on target (which averaged around 5 J); the maximum intensity was therefore about 10^{19} W cm^{-2}. The remaining part of the energy is distributed over a large spot (diameter about 40 μm), leading to an intensity in this region of about 10^{18} W cm^{-2}.

For the absorption measurements the targets were aluminium layers (0.9 μm thickness) evaporated on glass substrates and for the experiments concerning the suprathermal electrons the targets were combinations of thin metal foils (10 μm of $_{28}$Ni, 7.6 μm of $_{29}$Cu, and 15 μm of $_{30}$Zn). In both cases the targets were mounted on an xyz-translation stage in a vacuum chamber and the position could be controlled with an accuracy of 10 μm. The absorption measurements were performed at two different intensities for s- and p-polarized light and for a variety of angles of incidence. The fraction of the absorbed energy was determined by measuring (i) the fraction of backscattered light, (ii) the fraction of specular reflected light, and (iii) the fraction of diffuse reflected light. The diffuse reflected light was collected by an Ulbricht sphere (25 cm diameter, inner surface coated with $BaSO_4$). The linearity of the sphere was carefully checked prior to the measurements.

In order to characterize the bursts of suprathermal electrons produced during laser irradiation two detector arrangements were used. First was an electron spectrometer with six channels from 0.4 to 3 MeV. The energy window of each channel is about 100 keV [20]. After entering the spectrometer the electrons follow a circular trajectory corresponding to their momentum and are spatially separated at the plane of detection. The magnetic field (1700 G) is produced by a pair of permanent magnets and the entrance hole is covered by a 10-μm-thick aluminum foil in order to shield the detectors from light.

Second, a von Hamos spectrometer with cylindrically bent lithiumfluoride crystals (bending radius 100 mm) of (200) and (420) orientations was used to measure the $K\alpha$ emission of thin foil targets [21]. With the LiF crystals the $K\alpha$ lines from Ti ($Z=22$) to Ge ($Z=32$) could in principle be detected. The spectrometer was calibrated using the film calibration for Kodak-SB x-ray film and the calculated reflectivity data of LiF using kinetic diffraction theory. Although the reflectivity data are usually larger than the real reflectivity of LiF, the estimated photon numbers still provide a lower limit for the number of emitted photons. The detection limit of the spectrometer given by the film noise was about 3.0×10^{10} photons emitted into 4π per laser shot.

In addition to the above-mentioned detectors, two scintillator arrangements were used to measure the hard-x-ray radiation in the energy range of 60 keV up to about 1 MeV: a 3-mm-thick NaI scintillator crystal and a plastic scintillator, both coupled to photomultiplier tubes. The detectors were shielded against scattered x-ray radiation by a lead tube cover with a wall thickness of 0.5 cm. A wall of 5-cm-thick lead bricks was additionally built up in front of the detectors. Two 2.8-cm holes in the lead bricks in front of the detectors ensured that only directly incident radiation was detected. The scintillators were located 300 cm from the plasma source, approximately parallel to the target surface at normal incidence. The detectors were equipped with additional apertures with a 1.2-cm opening in a 2-cm-thick Tungsten piece, hence collecting a solid angle of 1.3×10^{-5} sr. One iron filter of 1.4 cm thickness in front of the NaI detector and a 1.4-cm iron plus 2-cm aluminum filter in front of the plastic detector attenuated the radiation in order to restrict the

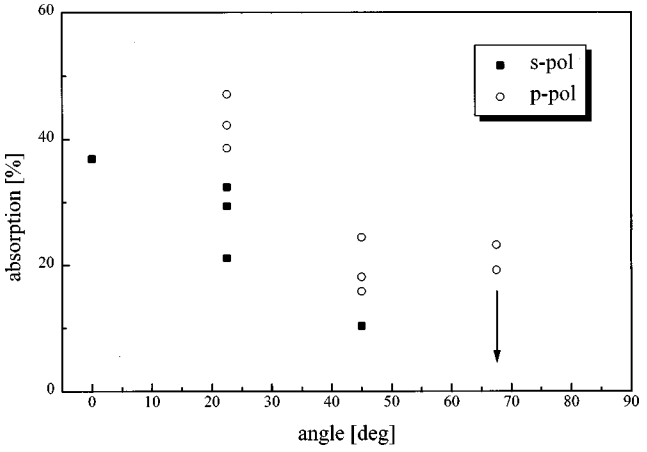

FIG. 2. Measured absorption as a function of the angle of incidence for *s*- and *p*-polarized light at an intensity of about 10^{19} W cm^{-2} in the center part of the focus.

response to a linear regime. The spectral sensitivities were calibrated in the range of 9 keV to 1.23 MeV using $K\alpha$ radiation from different materials (8.64, 15.75, 22.1, 35.86, 44.47, 55.38, 68.78, 74.23, and 97.14 keV) produced in an electron-beam-driven x-ray tube and a γ-ray $^{60}_{27}$Co standard. Filter transmissions were determined from the Veigele tables [23]. X rays below 60 keV are not transmitted through a 1.4-cm-thick iron filter and above 1 MeV the detection efficiency of the scintillators is drastically reduced, so that the detected photon energies are in the range of 60 keV to about 1 MeV. It was carefully checked that only x-ray radiation originating from the target was measured by the detectors. Since electrons emitted from the target have to pass a 2-cm BK7 window and at least a 1.4-cm iron filter their energy must be higher than about 50 MeV before they impinge on the detectors. First there are very few of such energetic electrons and second it is rather unlikely that these electrons then cause an event in the scintillator material.

III. RESULTS AND DISCUSSION

A. Absorption measurements

Although theoretical studies have been extended to ultrahigh intensities, to our knowledge no experimental investigations of laser pulse absorption as a function of the angle of incidence and the polarization have been performed at intensities in excess of 10^{19} W cm^{-2}and a contrast ratio of 10^{12}. Figure 2 shows the fraction of absorbed energy as a function of the angle of incidence for *s*- and *p*-polarized light at a normal incidence intensity of 10^{19} W cm^{-2}. It can be seen that the absorption for the different directions of polarization is only slightly different. The absorption peaks at 25° reaching values of about 40-45 % for *p*-polarized light. The value for 67.5° is an upper limit of the absorption since at this angle there was no opening in the Ulbricht sphere to measure the specularly reflected light, which was therefore impinging on the inner wall of the Ulbricht sphere. From calibration measurements it is known that the energy density then exceeds the linear range of the sphere. Therefore, the determined value of the reflected energy is too small and the absorption value is actually lower.

The peaking of the absorption at relatively small angles is in contrast to the results of one-dimensional models of the interaction of a high-intensity laser pulse with a steplike, highly overdense plasma interface, where the angle of maximum absorption is expected in the range of 45°–80° [13,15,16]. This and the fact that there is only a slight difference between *s*- and *p*-polarized light may be explained by the onset of surface irregularities as discussed in the Introduction. Variations in an originally flat surface reduce or even remove the distinction between *s*- and *p*–polarized light in the variation of absorption with incidence angle that is present at lower intensities [3,6,12]. On the scale of the surface variations there will be an admixture of angles with respect to the surface normal.

Evidence of laser-induced surface modification is also supported by Fig. 3, where the relative fraction of diffuse reflected light is displayed as a function of the incident laser intensity. The total reflected light is the sum of diffuse, specular, and backscattered components. The plot contains all data points measured at 22.5° and 45° for *s*- and *p*-polarized light. The fraction of the diffuse reflected light increases dramatically with intensity, a behavior that would be expected for an increasingly roughened surface or a surface that is strongly pushed inward by the ponderomotive pressure [7,14,24]. Using a simple estimate of the hole depth at the center of the focal spot and assuming that the modified surface acts like a hollow spherical dish, the fraction of the diffuse reflected light may be calculated as a function of the intensity. The depth in the center of the focal spot may be estimated as [18]

$$h = c\tau_L \sqrt{\frac{n_c}{2n_e}\frac{m_e Z}{m_i}\frac{I\lambda^2}{1.37\times 10^{18}}}, \tag{2}$$

where c is the speed of light, τ_L the pulse duration, n_e the electron density, n_c the critical electron density, Z the effective ionization degree, m_e the electron mass, m_i the ion mass, I the laser intensity in W cm^{-2}, and λ the laser wavelength in μm. The region between the two solid lines in Fig. 3 shows the result of such an estimate. The lower and the upper border lines correspond to an ion density equal to the solid state density of the bulk and to one-tenth of this value, respectively. The solid angle of the incoming laser light was determined by the f number of the focusing optics and the solid angle of the specular reflected component is identical to this value since it is determined by the opening in the Ulbricht sphere. The buckling of the surface now leads to a larger solid angle of the reflected light, therefore leading to a decrease of the measured specular reflected component determined by the opening in the Ulbricht sphere and an increase of the diffuse reflected light. From Fig. 3 it may be seen that there is qualitative agreement between the simple model and the experimental data.

B. Suprathermal electrons

Figure 4 shows the number of electrons emitted per solid angle detected by the electron spectrometer as a function of the energy. The target was 400-nm aluminum evaporated on a 7.6-μm copper foil. The angle of incidence was 0° and the electron spectrometer was oriented under an angle of 45°

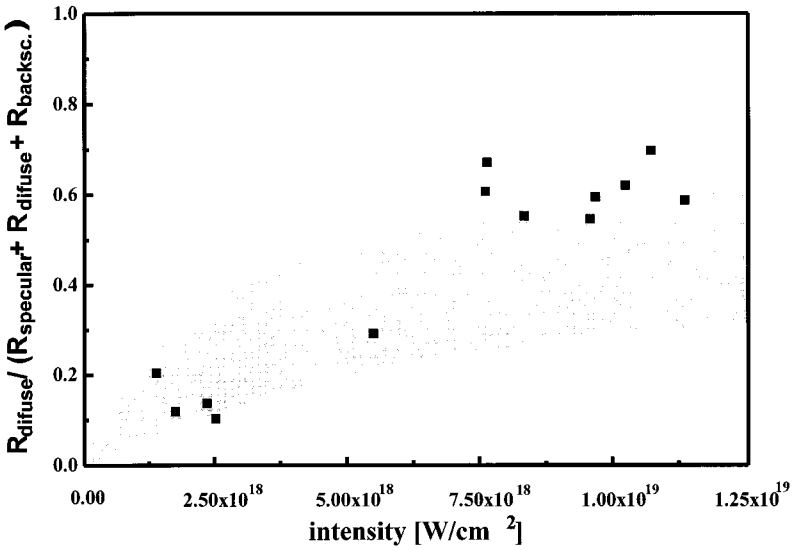

FIG. 3. Ratio of the diffuse to total (backscattered plus diffuse plus specular) reflected light. Due to surface modifications the specular reflected light decreases with intensity. The solid lines correspond to the ratio of diffuse to total reflected light if the surface modification acts as a spherical mirror. The lower and the upper lines are calculated for an ion density equal to solid-state density of the bulk and to one-tenth of this value, respectively.

with respect to the target normal observing from the back side. The intensity in the central spot was 4×10^{18} W cm^{-2}. Assuming an exponential electron distribution the temperature of the suprathermal electrons obtained from Fig. 4 is 420 keV, which is about 40% higher than what is expected from the naive scaling law [see Eq. 1]. The total number of electrons is about 10^9 sr^{-1} and the total energy carried by the electrons is estimated to 0.75 mJ. Hence the efficiency for the production of suprathermal electrons, with respect to the energy in the central spot, is on the order of 3×10^{-3}. The detection angle of the spectrometer has been varied between 0° and 45°, but no significant difference either in electron energy or in the total number of electrons has been found.

In order to characterize the suprathermal electrons by detecting the $K\alpha$ emission of multilayer targets [17,25–27] the following target combinations have been used: Ni-Cu-Zn, Zn-Ni-Cu, Cu-Zn, and Cu. The basic idea is that the electrons penetrate the first layer, lose part of their kinetic energy, and then penetrate the second (third) layer. In all layers, inner-shell ionization by electron impact occurs. By measuring the intensity of the $K\alpha$ emission originating from the first, the second, and the third layer as a function of the thickness of the top layer, the energy of the electrons and the number of electrons can be deduced [25,17]. In practice, the experimental results were compared to simulations that consider the $K\alpha$ line production by electrons penetrating the target with energies from 10 keV up to 1 MeV. The energy loss of the electrons was calculated using the Bethe formula and the $K\alpha$ x-ray production was determined using the K-shell cross sections from [28]. The relative line intensities ($K\alpha$ series) as well as the fluorescence yields were taken from [29]. It should be mentioned that the calculated conversion efficiency from electron energy to x-ray energy is in very good agreement with the experimental data for solid targets used in electron microscopy [30].

For all target combinations only the $K\alpha$ line radiation originating from the top layer has been observed. Their photon energies are 7.4781 keV (Ni $K\alpha$), 8.0478 keV (Cu $K\alpha$), and 8.6389 keV (Zn $K\alpha$), respectively. Although the excitation energy of the K shell of the three elements is different, for all lines the number of photons emitted from the target was on the order of $(1.1\pm0.4)\times10^{12}$ photons per shot. Due to the fact that no $K\alpha$ line radiation from the second or third layer was observed and assuming that the electrons were penetrating almost perpendicularly with respect to the target surface, the energy of the electrons producing the major part of the x-ray photons is lower than 60 keV (top layer: Cu) or 90 keV (top layer: Ni). It should be mentioned that the number of electrons with higher energies (between 400 keV and 900 keV), which were observed with the electron spectrometer, is too low to produce enough photons that could be detected with the von Hamos spectrometer. Even if one assumes that the detected electrons belong to the high-energy wing of an exponential electron distribution with a temperature of 420 keV, their number is too small to produce a

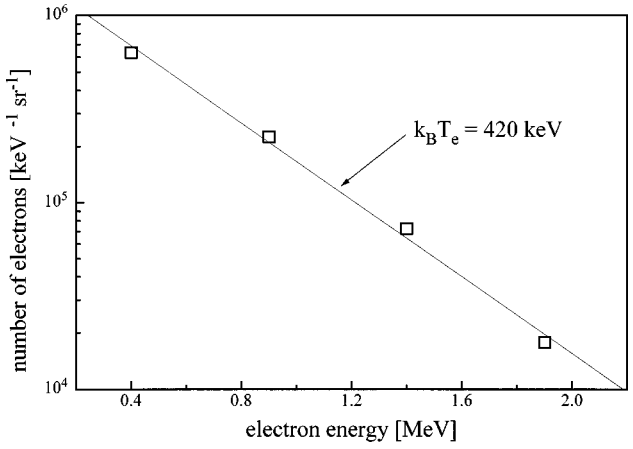

FIG. 4. Numbers of electrons as a function of the energy. From the slope of the curve an electron temperature of 420 keV can be derived. The target was 400-nm aluminum on 7.6-μmcopper foil and the intensity was 4×10^{18} W cm^{-2}.

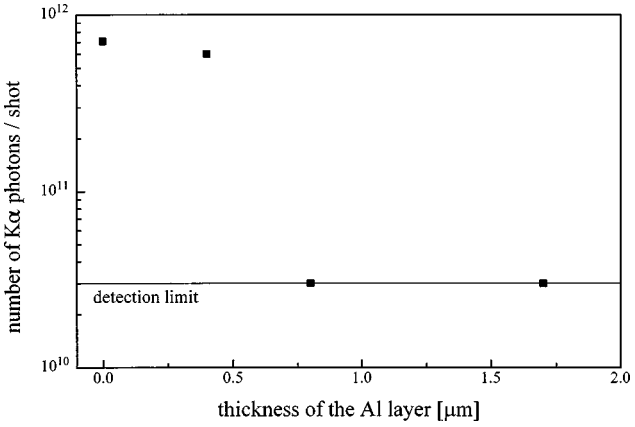

FIG. 5. Copper $K\alpha$ intensity as a function of the thickness of the top aluminum layer. For aluminum layers thicker than about 800 nm no copper $K\alpha$ signal can be detected.

detectable signal. Taking into account an average conversion efficiency of $\eta=0.8\%$ (for the conversion of electrons between 10 keV and 90 keV to $K\alpha$ photons), as found in the simulation, the number of electrons produced per laser shot is on the order of $N_H\simeq(1.4\pm0.5)\times10^{14}$. This result might be explained by the fact that about 85% of the laser energy has been focused to an intensity of about 10^{18} W cm^{-2}, producing electrons with a temperature much lower than the ones detected by the electron spectrometer.

In order to further characterize the electrons contributing to the $K\alpha$ production by electron impact, targets consisting of two layers, namely, aluminum (100–1700 nm) on copper (7.6 μm), were used. The Cu $K\alpha$ intensity was recorded as a function of the thickness of the aluminum layer. Figure 5 shows that for aluminum layers thicker than about 0.5 μm no Cu $K\alpha$ radiation can be detected. This result would be consistent with the simulations only if the temperature of the electrons is lower than 15 keV. But in this case the conversion efficiency into $K\alpha$ radiation is extremely small and in order to produce the observed number of $K\alpha$ photons a conversion efficiency of laser energy to electron energy in excess of 100% would be neccessary. Therefore, the electrons must have a higher energy and the transport to a depth of more than about 1 μm is *inhibited* either by lateral transport or by some flux limitation mechanism.

The effect of lateral transport of suprathermal electrons produced in laser-plasma experiments has been studied previously by a number of authors in the context of nanosecond laser-plasma interactions [31–33]. Suprathermal electrons that are mostly accelerated perpendicular to the target surface induce a toroidal magnetic field that is oriented symmetrically to the target normal. In all of these works, electrodynamic simulations showed that the electron trajectories have lateral extensions along the target surface up to hundreds of micrometers depending on the strength of the magnetic field. These theoretical results were qualitatively confirmed in earlier experiments by Kieffer *et al.* [34,35] and Luther-Davies *et al.* [36], who analyzed the angular dependence of the bremsstrahlung and K_α radiation and the lateral spatial x-ray emission originating from suprathermal electrons produced with CO_2 and Nd:glass lasers. In contrast to the experiments in Refs. [34–36], where $I\lambda^2<10^{15}$ W cm^{-2} μm^2, the present investigation was performed at much higher intensities. The average current carried by the keV electrons over the pulse duration $\tau=300$ fs is around $I_H=eN_H/\tau\simeq75$ MA. The resulting magnetic field at the perifery of the low-intensity spot (~40 μm) would be $\sim4\times10^9$ G, which is much higher than the 10^6-G fields typical for long-pulse interactions [32,33]. Taking into account that the electrons should have an anisotropic velocity distribution with a strong component parallel to the target surface, the energy loss will occur in a much thinner layer than expected for perpendicular penetration. Thus the extracted temperature is larger than 15 keV and the conversion efficiency of laser energy to electron energy would be on the order of the observed values.

The stopping of electrons by means other than collisions with bulk atoms could also be explained by the buildup of electrostatic fields. As Bell *et al.* have pointed out recently [37], a gigagauss magnetic field carried into the target over a typical electron stopping distance is energetically impossible since it would store a magnetic energy orders of magnitude larger than the absorbed laser energy. The hot-electron current must therefore be locally canceled by a return current. For a target with finite conductivity, however, it may not be possible to balance a current of about 10^7 A in several hundred femtoseconds. On the other hand, the resulting charge separation will lead to the formation of large electrostatic fields, thus slowing down the electrons and giving an effective stopping distance R_H of [37]

$$R_H=\left(\frac{T_H}{100\,\mathrm{keV}}\right)^2\left(\frac{\sigma}{10^6\,\Omega^{-1}\,\mathrm{m}^{-1}}\right)\left(\frac{I_a}{10^{18}\,\mathrm{W\,cm}^{-2}}\right)^{-1}3\ \mu\mathrm{m}, \tag{3}$$

where σ is the conductivity of the target material and $I_a=\eta_H I$ is the ''absorbed intensity'' into hot electrons. For solid aluminium at temperatures up to 100 eV, we have $\sigma\sim10^6\,\Omega^{-1}\,\mathrm{m}^{-1}$ [4]. Taking $I_a=10^{18}$ W cm^{-2} μm^{2}and $T_H=50$ keV, we find that the electrons are stopped in a characteristic distance of $R_H\simeq0.75$ μm, considerably less than the range expected from the Bethe formula. This value is consistent with the results displayed in Fig. 5 given the uncertainty ($\times5$) in determining the intensity of the region surrounding the central spot.

Summarizing the measurements and the analysis concerning the suprathermal electrons, it can be stated that in the central focal spot about 10^{10} electrons with a characteristic temperature of 420 keV are generated, whereas in the surrounding region about 10^{14} electrons with several tens of keV are produced. The current associated with the large number of ''low''-energy electrons creates enormous magnetic and electrostatic fields, which inhibit the perpendicular penetration into the bulk material behind the plasma layer either by adding velocity components parallel to the target surface or by stopping the electrons due to the large electrostatic force.

C. Hard-x-ray radiation

Aluminum layers evaporated on a glass substrate were used as targets. The results obtained with both detectors yielded an averaged total energy of hard x-rays of several μJ in the mentioned energy range (60 keV to 1 MeV). This corresponds to a conversion efficiency of the incident laser

è TABLE I. Measured efficiencies for hard-x-ray production using various laser systems.

Laser	Wavelength (nm)	Polarization	Intensity (W cm^{-2})	Pulse length (fs)	X rays	Efficiency	Target	Reference
Nd:glass	532	*s*	2×10^{19}	300	60 keV–1 MeV	10^{-4}	Al	present work
Ti:sapphire	807	*p*	3×10^{18}	120	$>$ 30 keV	3×10^{-3}	Ta	[38]
						5.7×10^{-4}	Al	
Nd:glass	1053	*p*	7×10^{17}	1500–2500	$>$ 50 keV	2.6×10^{-3}	Ta	[7]

energy in the central spot into hard x-rays of about 10^{-6}. The efficiency was derived under the assumptions of an isotropic radiating source and a Maxwellian velocity distribution of the suprathermal electrons in the plasma with a characteristic temperature of 420 keV as measured with the electron spectrometer.

The energy coupling into hard x-rays is several orders of magnitude lower compared to other experimental results, which are summarized in Table I. Kmetec *et al.* reported a conversion efficiency of 5.7×10^{-4} for aluminum targets [38]. These investigations were done at a lower intensity of 10^{18} W cm^{-2}with a 0.5-TW Ti:sapphire laser. Using a scaling of the x-ray yield with the 3/2 power of the incident laser energy [38], one would expect for aluminum a conversion efficiency of 10^{-3} for an intensity of 10^{19} W cm^{-2}. Other investigations yielded similar values for the conversion into hard x rays (see Table I). The hard-x-ray emission is due to bremsstrahlung from suprathermal electrons decelerated in the solid behind the plasma. Usually the velocity distribution of the suprathermal electrons can be characterized in the case of a Maxwellian distribution by a single parameter T_H (given in eV units). The conversion efficiency η from electron kinetic energy E_k into energy E_x of bremsstrahlung radiation can be estimated for a Maxwell distribution according to [39] with $\eta=E_x/E_k=1.65\times10^{-9}ZV$, where Z is the atomic number and V is the kinetic electron energy in eV units. For aluminum ($Z=13$) and a characteristic temperature of 420 keV this yields an efficiency of $\eta=0.9\%$ for the bremsstrahlung production. Therefore, only about 10^{-4} of the laser energy contained in the central spot is converted into suprathermal electrons. Within an order of magnitude this is consistent with the results obtained with the electron spectrometer. The comparatively low conversion efficiency may be a consequence of the extremely high contrast ratio of the laser pulse and the generation of large magnetic fields, inhibiting an efficient energy coupling into hot electrons.

IV. CONCLUSION

It has been verified experimentally that even at peak intensities of 10^{19} W cm^{-2}the coupling of laser energy into the plasma reaches values of about 45%. The marginal difference between *s*- and *p*-polarized light and the fact that the specular reflected light decreases significantly with increasing laser intensity indicate that modifications in the surface morphology, consistent with hole boring, become important. The investigations of the suprathermal electrons using an electron spectrometer and the measurement of the hard-x-ray emission yield a conversion efficiency from laser energy to electron energy of 10^{-4}–10^{-3}. These electrons, with a temperature on the order of 400 keV, are produced in the central focal spot that contains about 15% of the full laser energy. Approximately 85% of the laser energy is focused to an intensity of about 10^{18} W cm^{-2}, leading to about 10^{14} low-energy electrons (several tens of keV). The measurements indicate that these electrons either have a strong velocity component parallel to the target surface or are decelerated by strong electrostatic fields. Even though the present investigation has been restricted to ''cold,'' high-density targets, the low conversion efficiency measured into MeV electrons may equally apply to the hot, compressed plasma in the fast ignitor scheme.

ACKNOWLEDGMENTS

The authors would like to thank the P102 laser staff. This work was supported by the European Community (Contract No. CHGE.CT920016).

[1] M. Tabak, J. Hammer, M. E. Glinsky, W. L. Kruer, S. C. Wilks, J. Woodworth, E. M. Campbell, M. D. Perry, and R. J. Mason, Phys. Plasmas **1**, 1626 (1994).
[2] M. M. Murnane, H. C. Kapteyn, M. D. Rosen, and R. W. Falcone, Science **25**, 531 (1991).
[3] R. Fedosejevs, R. Ottmann, R. Sigel, G. Kühnle, S. Szatmari, and F. P. Schäfer, Phys. Rev. Lett. **64**, 1250 (1990).
[4] H. M. Milchberg, R. R. Freeman, S. C. Davey, and R. M. More, Phys. Rev. Lett. **61**, 2364 (1988).
[5] U. Teubner, J. Bergmann, B. van Wonterghem, F. P. Schäfer, and R. Sauerbrey, Phys. Rev. Lett. **70**, 794 (1993).
[6] J. C. Kieffer, M. Chaker, J. P. Matte, H. Pepin, Y. Cote, Y. Beaudoin, T. W. Johnston, C. Y. Chien, S. Coe, G. Mourou, and O. Peyrusse, Phys. Fluids B **5**, 2330 (1993).
[7] M. Schnürer, M. P. Kalashnikov, P. V. Nickles, Th. Schlegel, W. Sandner, N. Demchenko, R. Nolte, and P. Ambrosi, Phys. Plasmas **2**, 3106 (1995).
[8] D. F. Price, R. M. More, R. S. Walling, G. Guethlein, R. L. Shepherd, R. E. Stewart, and W. E. White, Phys. Rev. Lett. **75**, 252 (1995).
[9] F. Brunel, Phys. Rev. Lett. **59**, 52 (1987).
[10] S. C. Rae and K. Burnett, Phys. Rev. A **44**, 3835 (1991).
[11] P. Gibbon and A. R. Bell, Phys. Rev. Lett. **68**, 1535 (1992).
[12] R. P. Godwin, Appl. Opt. **33**, 1063 (1994).

[13] P. Gibbon, Phys. Rev. Lett. **73**, 664 (1994).
[14] U. Teubner, P. Gibbon, E. Förster, F. Fallies, P. Audebert, J. P. Geindre, and J. C. Gauthier, Phys. Plasmas **3**, 2679 (1996).
[15] A. A. Andreev, E. G. Gamalii, V. N. Novikov, A. N. Semakhin, and V. T. Tikhonchuk, Zh. Éksp. Teor. Fiz. **101**, 1808 (1992) [Sov. Phys. JETP **74**, 963 (1992)].
[16] H. Ruhl and P. Mulser, Phys. Lett. A **205**, 388 (1995).
[17] U. Teubner, I. Uschmann, P. Gibbon, D. Altenbernd, E. Förster, T. Feurer, W. Theobald, R. Sauerbrey, G. Hirst, M. H. Key, J. Lister, and D. Neely, Phys. Rev. E **54**, 4167 (1996).
[18] S. C. Wilks, W. L. Kruer, M. Tabak, and A. Langdon, Phys. Rev. Lett. **69**, 1383 (1992).
[19] B. Quesnel, P. Mora, J. C. Adam, S. Guerin, A. Heron, and G. Laval, Phys. Rev. Lett. **78**, 2132 (1997).
[20] G. Malka and J. L. Miquel, Phys. Rev. Lett. **77**, 75 (1996).
[21] U. Teubner, T. Miβalla, I. Uschmann, E. Förster, W. Theobald, and C. Wülker, Appl. Phys. B **62**, 213 (1996).
[22] N. Blanchot, C. Rouyer, S. Sauteret, and A. Migus, Opt. Lett. **20**, 395 (1995).
[23] W. J. Veigele, At. Data **5**, 51 (1973).
[24] R. Sauerbrey, Phys. Plasmas **3**, 4712 (1996).
[25] J. D. Hares, J. D. Kilkenny, M. H. Key, and J. G. Lunney, Phys. Rev. Lett. **42**, 1216 (1979).
[26] C. Rousseaux, F. Amiranoff, C. Labaune, and G. Mathieussent, Phys. Fluids B **4**, 2589 (1992).
[27] A. Rousse, P. Audebert, J. P. Geindre, F. Fallies, J. C. Gauthier, A. Mysyrowicz, G. Grillon, and A. Antonetti, Phys. Rev. E **50**, 2200 (1994).
[28] E. Casnati, A. Tartari, and C. Baraldi, J. Phys. B **15**, 155 (1982).
[29] G. Zschornack, *Atomdaten für die Röntgenspektralanalyse* (Deutscher-Verlag für Grundstoffindustrie, Leipzig, 1989).
[30] M. Greena and V. E. Cosslett, Br. J. Appl. Phys., J. Phys. D **2**, 425 (1968).
[31] D. W. Forslund and J. U. Brackbill, Phys. Rev. Lett. **48**, 1614 (1982).
[32] R. Fabbro and P. Mora, Phys. Rev. Lett. **90A**, 48 (1982).
[33] J. Wallace, Phys. Rev. Lett. **55**, 707 (1985).
[34] J. C. Kieffer, H. Pepin, M. Pich, J. P. Matte, T. W. Johnston, P. Lavigne, F. Martin, and R. Decoste, Phys. Rev. Lett. **50**, 1054 (1983).
[35] J. C. Kieffer, H. Pepin, and F. Amiranoff, Appl. Phys. Lett. **44**, 494 (1984).
[36] B. Luther-Davies, A. Perry, and K. A. Nugent, Phys. Rev. A **35**, 4306 (1987).
[37] A. R. Bell, J. R. Davies, S. Guérin, and H. Ruhl, Plasma Phys. Control Fusion **39**, 653 (1997).
[38] J. D. Kmetec, C. L. Gordon III, J. J. Macklin, B. E. Lemoff, G. S. Brown, and S. E. Harris, Phys. Rev. Lett. **68**, 1527 (1992).
[39] G. H. McCall, J. Phys. D **15**, 823 (1982).